



Clot Analog Attenuation in Non-contrast CT Predicts Histology: an Experimental Study Using Machine Learning

Aglae Velasco Gonzalez¹ · Boris Buerke¹ · Dennis Görlich² · Manfred Fobker³ · Thilo Rusche¹ · Cristina Sauerland² · Norbert Meier⁴ · Astrid Jeibmann⁵ · Ray McCarthy⁶ · Harald Kugel⁴ · Peter Sporns¹ · Andreas Faldum² · Werner Paulus⁵ · Walter Heindel¹

Received: 14 October 2019 / Revised: 1 December 2019 / Accepted: 4 December 2019 / Published online: 14 January 2020
© Springer Science+Business Media, LLC, part of Springer Nature 2020

Abstract

Exact histological clot composition remains unknown. The purpose of this study was to identify the best imaging variables to be extrapolated on clot composition and clarify variability in the imaging of thrombi by non-contrast CT. Using a CT-phantom and covering a wide range of histologies, we analyzed 80 clot analogs with respect to X-ray attenuation at 24 and 48 h after production. The mean, maximum, and minimum HU values for the axial and coronal reconstructions were recorded. Each thrombus underwent a corresponding histological analysis, together with a laboratory analysis of water and iron contents. Decision trees, a type of supervised machine learning, were used to select the primary variable altering attenuation and the best parameter for predicting histology. The decision trees selected red blood cells (RBCs) for correlation with all attenuation parameters ($p < 0.001$). Conversely, maximum attenuation on axial CT offered the greatest accuracy for discriminating up to four groups of clot histology ($p < 0.001$). Similar RBC-rich thrombi displayed variable imaging associated with different iron ($p = 0.023$) and white blood cell contents ($p = 0.019$). Water content varied among the different histologies but did not in itself account for the differences in attenuation. Independent factors determining clot attenuation were the RBCs ($\beta = 0.33$, CI = 0.219–0.441, $p < 0.001$) followed by the iron content ($\beta = 0.005$, CI = 0.0002–0.009, $p = 0.042$). Our findings suggest that it is possible to extract more and valuable information from NCCT that can be extrapolated to provide insights into clot histological and chemical composition.

Keywords Blood clot · Helical CT · Red blood cells · Decision trees · Iron

Electronic supplementary material The online version of this article (<https://doi.org/10.1007/s12975-019-00766-z>) contains supplementary material, which is available to authorized users.

✉ Aglae Velasco Gonzalez
Aglae.VelascoGonzalez@ukmuenster.de

Boris Buerke
buerkeb@uni-muenster.de

Dennis Görlich
Dennis.Goerlich@ukmuenster.de

Manfred Fobker
Manfred.Fobker@ukmuenster.de

Thilo Rusche
Thilo.Rusche@ukmuenster.de

Cristina Sauerland
cristina.sauerland@ukmuenster.de

Norbert Meier
norbert.meier@uni-muenster.de

Astrid Jeibmann
Astrid.Jeibmann@ukmuenster.de

Ray McCarthy
rmccart9@ITS.JNJ.com

Harald Kugel
Kugel@uni-muenster.de; Harald.Kugel@ukmuenster.de

Peter Sporns
Peter.Sporns@ukmuenster.de

Andreas Faldum
Andreas.Faldum@ukmuenster.de

Werner Paulus
paulusw@uni-muenster.de

Walter Heindel
heindel@uni-muenster.de

Extended author information available on the last page of the article

Abbreviations

NCCT	Non-contrast CT
RBCs	Red blood cells
HU	Hounsfield units
ROI	Region of interest
WBCs	White blood cells
SD	Standard deviation
IQR	Interquartile range
AIS	Acute ischemic stroke

Introduction

Indications for endovascular treatment in acute ischemic stroke are based not only on clinical aspects but also on brain imaging [1–5]. Hence, multimodal brain CT, including non-contrast CT (NCCT), CT angiography, and CT perfusion, are widely used for diagnosis and in selecting patients for therapy.

Recent past studies have shown an association between clot dissolution and IV thrombolysis, especially for hyperdense clots on NCCT [6, 7]. Hyperdense clots are usually, but not always, rich in red blood cells (RBCs) and can usually be removed endovascularly [8–12]. In contrast, isodense clots, detected by NCCT in up to 75% of angiographic occlusions, are the most difficult to treat either pharmacologically or endovascularly and have been correlated with a high fibrin content [6, 13, 14]. Despite treatment, persistent thrombi are not available for examination of their histological features, and in such cases, clot imaging is the only resource for characterization. While clot composition is not currently considered in treatment decision making, it has been speculated that if composition could be known before treatment, it might then play a role in selecting the best endovascular strategy for therapy. Nevertheless, enhanced mechanical thrombectomy decision making before initiating intervention can only become a reality if thrombus characterization by diagnostic imaging improves. The potential to extrapolate clot imaging into histological information will represent a huge step in selecting optimized individualized stroke therapies. This could allow optimization of clot removal techniques and devices, facilitating more successful and shorter interventions and reducing the associated radiation and costs [15, 16].

To extract the maximum information on clot attenuation by NCCT, the measurement methodology and selected parameters must be analyzed. Thinner reconstructions offer greater accuracy for Hounsfield unit (HU) measurements of intracranial clots [14, 17, 18]. The question arises whether the commonly used mean HU represents the ideal parameter for extrapolating NCCT data into histology [12, 13, 17]. In addition, a better understanding is required of the relationship between different histological clot components and X-ray absorption in combination with other “overlooked” blood components such

as water or iron, which could affect both attenuation and MRI signal intensity in stroke imaging.

Clot analogs from real blood are the best alternative for the controlled production of human acute ischemic stroke (AIS) thrombi which allow repeatability in clots at discrete points over the wide compositional range of human thrombi. Such analogs are commonly accepted in the field, and they have been used in several *in vitro* investigations and in the pre-clinical testing of clot extraction devices for mechanical thrombectomy [19–22]. They have sought to simulate, but have not yet replicated, the complexity of *in vivo* thrombi, demonstrating less intraclot type variation than occurs in human AIS thrombi [23, 24]. Nevertheless, this homogeneity can be viewed as an essential advantage for studies like ours since every part of the thrombus can be a representative example for the whole. Our aim has been to take an in-depth look at clot composition and its relationship to X-ray absorption.

Thus, covering a wide range of histologies with clot analogs, we examined the histological component (RBCs, fibrin, and white blood cells) that correlates best with different NCCT parameters (maximum, minimum, or mean HU value) to determine attenuation cut-offs capable of predicting histology. Additionally, we analyzed the water and iron contents of clots together with their histological features in an effort to identify the main factors altering attenuation.

Methods

Generalities

Clot analogs of different but predefined composition were analyzed regarding X-ray attenuation on NCCT by applying the usual stroke protocol for patients. In each of the 80 clots evaluated with NCCT, the histological (RBCs, white blood cells (WBCs), and fibrin) and laboratory analyses (water and iron content) were correlated with the images. NCCT was performed at 24 and 48 h from clot production (Fig. 1). After production, clots were stored at 3 °C.

Clot Production

Thrombi were produced by Cerenovus from ovine venous blood [24]. Two production methods were used: manual contraction and platelet-driven contraction. The final content of RBCs in clots was assessed by mixing RBCs with plasma in various concentrations. The hematocrit of the blood mixtures before clotting was as follows: 84%, 20%, 5%, 1%, and 0 for the platelet contraction group, and 20%, 5%, 1%, and 0 for the manual contraction group. Further details are presented in the [Supplemental materials \(Methods\)](#).

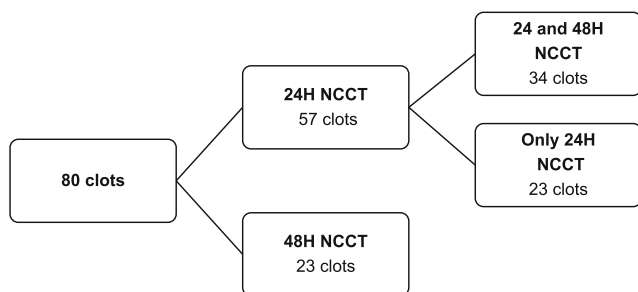


Fig. 1 Clot imaging flow chart

Histological Analysis

Thrombus material from each of the clots examined by NCCT was immediately fixed in 10% phosphate-buffered formalin. The formalin-fixed clot was embedded in paraffin, cut in 5- μ m thick slices, and stained with hematoxylin and eosin and Martius scarlet blue (differentiating fibrin and RBCs). Two of the authors (AJ, senior neuropathologist, and AVG, neuroradiologist) carried out the histological evaluation. Using $\times 40$ magnification, clot cores were photographed (Olympus BX43 microscope + digital camera). ImageJ software (version 1.52a) was used for the quantitative threshold-based automatic measurement of the percentage fibrin, RBCs, and WBCs.

Clinical Laboratory Analysis

Water content was determined by drying the samples at 90 °C using the standard protocol. Iron(III) was measured by spectrometry. A detailed protocol of these analyses is included in the [Supplemental material \(Methods\)](#).

Specimen Preparation and Non-contrast CT Protocol

Before imaging, every thrombus was placed in a single 5-mL Eppendorf tube with 2% agarose. Each thrombus was fixed centrally inside the Eppendorf tubes, avoiding the presence of air. The tubes were placed in a Plexiglass holder which was immersed in a plastic container filled with 2.5 L of water (see Supplemental materials, Figure 1: clot phantoms). In all cases, the phantom was placed at the isocenter of the CT gantry. All clots underwent a 0.4-mm axial non-contrast scan (Somatom Definition Flash, Siemens Healthineers) at the following parameters: pitch 0.55, 125 kVp, 300 mA, rotation time 1 s, caudocranial direction. Image reconstruction was 1-mm slice thickness, kernel H10s, and 1-mm axial and coronal reconstructions were used to measure the clot attenuation.

Imaging Analysis and Measurements

Through consensus, two authors (AGV, senior neuroradiologist, and TR, assistant radiologist) placed regions of interest (ROIs) within the clots. Measurements at the thrombus-

agarose or thrombus-plastic tube interface were avoided in all cases. Circular ROIs with a minimum square of 5 mm² were used for axial reconstructions, and irregular ROIs of at least 40 mm² for coronal reconstructions. For every axial and coronal ROI, the following values of attenuation were recorded: mean, maximum, and minimum Hounsfield units (six different attenuation parameters per ROI). The background noise was ± 5 HU (quality assurance by water phantom).

Statistical Analysis

All statistical analyses were performed using the SPSS version 25/2017 software (IBM). p values ≤ 0.05 were deemed to indicate a statistically significant difference. All reported p values were two sided. Continuous variables have been described in terms of the mean, standard deviation (SD), median, interquartile range (IQR), and range. The Mann-Whitney U test was used to test the differences in the continuous variables. The relationships between attenuation, histology, and laboratory results were tested using the Spearman correlation (Spearman ρ). Different regression models were compared to identify suitable mathematical models for the association between attenuation and the histology and laboratory analysis variables. The linear model is presented here for reference with the cubic regression results that had the best fit among the different models tested. Results have been presented using the coefficient of determination (R^2) and the regression coefficients (β).

Decision trees were used to decide which histological feature was best associated with all the different attenuation parameters at 24 h. The same methodology was used to identify the best attenuation parameter (among the mean, minimum, and maximum HU values) to determine cut-offs for histological prediction. The settings of the decision trees were as follows: maximum depth = 1, minimum splitting size = 10, minimum child size = 5, tenfold cross-validation, alpha = 0.05, maximum split number = 4. This analysis was Bonferroni-adjusted. Changes in attenuation between 24 and 48 h were compared using the Wilcoxon signed-rank test and also analyzed by a generalized linear mixed model with repeated measurements together with RBCs, WBCs, iron, and water.

Results

General Results

The results are presented for the total clots analyzed ($n = 80$) unless specified otherwise.

Histological Analysis

The median RBC content of the 80 thrombi was 69.9% (IQR = 25.9–92.2, range (0–99.9), mean = 58.2 ± 37.3), fibrin

30% (IQR = 7.5–74.1, range (0–100), mean = 41.6 ± 37.4), and WBCs 0.11% (IQR = 0.01–0.24, range (0–0.98), mean = 0.14 ± 0.15). There was a significant inverse correlation between the percentage RBCs and fibrin (Spearman $\rho = -0.997$, $p < 0.001$). Clots with a higher WBC count correlated with lower fibrin (Spearman $\rho = -0.629$, $p < 0.001$) and higher RBC contents (Spearman $\rho = 0.599$, $p < 0.001$).

Laboratory Analysis

The median iron concentration was 992 $\mu\text{g/g}$ (IQR = 423–1655, range (9–3057), mean = 1118 ± 848), and water content (percentage of loss of weight before and after drying) was 70.5% (IQR = 46.5–83.8%, range (14.3–89.5), mean = 65.6 ± 19.4). Thrombi with more RBCs correlated with a higher iron content (Spearman $\rho = 0.792$, $p < 0.001$) and less water (Spearman $\rho = -0.624$, $p < 0.001$). Linearly, for every 1% of RBCs, the iron concentration increased by 17.8 $\mu\text{g/g}$ ($R^2 = 0.615$, $p < 0.001$), and the percentage water decreased by 0.26% ($R^2 = 0.248$, $p < 0.001$). In the [Supplemental materials](#), [Figure 2](#) illustrates the relationship of RBCs with iron and water contents.

Imaging Analysis

For the attenuation analysis of the clots, a total of 160 ROIs were placed. [Table 1](#) in the [Supplemental materials](#) sets forth the mean, maximum, and minimum HU for the axial and coronal CT reconstructions at 24 and 48 h.

Decision Tree Analysis

Machine learning trees were developed, all with the same methodology, to ascertain which histological component could best be classified radiologically and vice versa. First, to determine which histological component could best be classified radiologically, we developed decision trees (24 h clots, $n = 57$) with RBC, fibrin, WBC, iron, and water contents as independent covariates and the mean, maximum, and minimum HU values in the axial and coronal reconstructions as separate dependent variables (six decision trees, one for each attenuation parameter). The results of the decision trees were identical. In all cases, the RBCs correlated best with each of the six HU parameters ($p < 0.001$). More specifically, the resulting optimal RBC cut-offs were (1) $\leq 68.35\%$, (2) 68.35–94.4%, and (3) $> 94.4\%$ RBC.

By contrast, to analyze which of the six attenuation parameters offered the greatest accuracy in determining the RBC content, we developed a new decision tree with RBCs as the dependent variable (24 h clots, $n = 57$). The maximum attenuation values for thrombi on axial NCCT were found to correlate best with the percentage of RBCs. The attenuation cut-offs located at ≤ 43 HU, 43–60 HU, 60–75 HU, and > 75 HU corresponded to mean RBC values of 14%, 37%, 85%, and 96%, respectively ($p < .001$). [Figure 2](#) depicts this decision tree and the

histological and radiological correlations. [Figure 3](#) illustrates our explanation for why the maximum attenuation values were selected best predictors over the rest of the attenuation parameters: the maximum attenuation was more consistent with characterization of the material when changes in ROI position or size occurred. The following analysis therefore focuses on the factors influencing the maximum HU values on axial NCCT.

Factors Altering Clot Attenuation

Joint Analysis of Histology and Chemical Clot Composition

High clot attenuation was correlated with a higher proportion of RBCs (Spearman $\rho = 0.894$, $p < 0.001$), WBCs (Spearman $\rho = 0.608$, $p < 0.001$), and iron content (Spearman $\rho = 0.776$, $p < 0.001$). Lower attenuations were correlated with high fibrin (Spearman $\rho = -0.897$, $p < 0.001$) and water contents (Spearman $\rho = -0.566$, $p < 0.001$). The scatter plots for the above-mentioned variables with regard to maximum attenuation values on axial CT are shown in [Fig. 4](#), and [Table 1](#) lists the factors for predicting clot attenuation when linear models and cubic models were used for reference.

Mathematically, the greater the percentage RBCs, the higher the HU value. Nevertheless, there was a subgroup of clots with nearly 100% RBCs but significantly different attenuations ($p < 0.001$). [Table 2](#) summarizes the features of these hyperdense clots, divided into two groups (group 1 = ≤ 80 axial maximum HU and group 2 = > 80 axial maximum HU, total $n = 20$). With similar RBC ($p = 0.16$) and water contents ($p = 0.91$), group 2 exhibited higher iron content and percentage WBCs ($p = 0.023$ and $p = 0.019$, respectively).

A generalized linear mixed model with repeated measurements (114 measurements on 23 clots at 24 h, 23 clots at 48 h, and 34 clots at 24 and 48 h) for maximum HU values on axial CT as the dependent variable revealed that the RBC content was the most important factor influencing attenuation ($\beta = 0.33$, CI = 0.219–0.441, $p < 0.001$), followed by the iron content ($\beta = 0.005$, CI = 0.0002–0.009, $p = 0.042$). The percentage of total water in the clot ($\beta = -0.01$, CI = -0.143–0.124, $p = 0.89$) and the WBCs ($\beta = 7.637$, CI = -8.942–24.217, $p = 0.36$) did not show any significant effect in this multivariate analysis.

Changes in Attenuation over Time

In general, clots decreased attenuation over time, though it also increased in a minority. In the [Supplemental materials](#), [Figure 3](#) presents the changes in attenuation for the maximum attenuation values on axial CT by the decision tree groups for RBCs. Although in the univariate analysis there were no significant attenuation differences on clots at 24 h vs. 48 h ($p = 0.072$), repeated measurement analysis of this last multivariable showed a statistically significant decrease of 1.891 HU between 24 h and 48 h (CI = 0.016–3.767, $p = 0.048$), thus

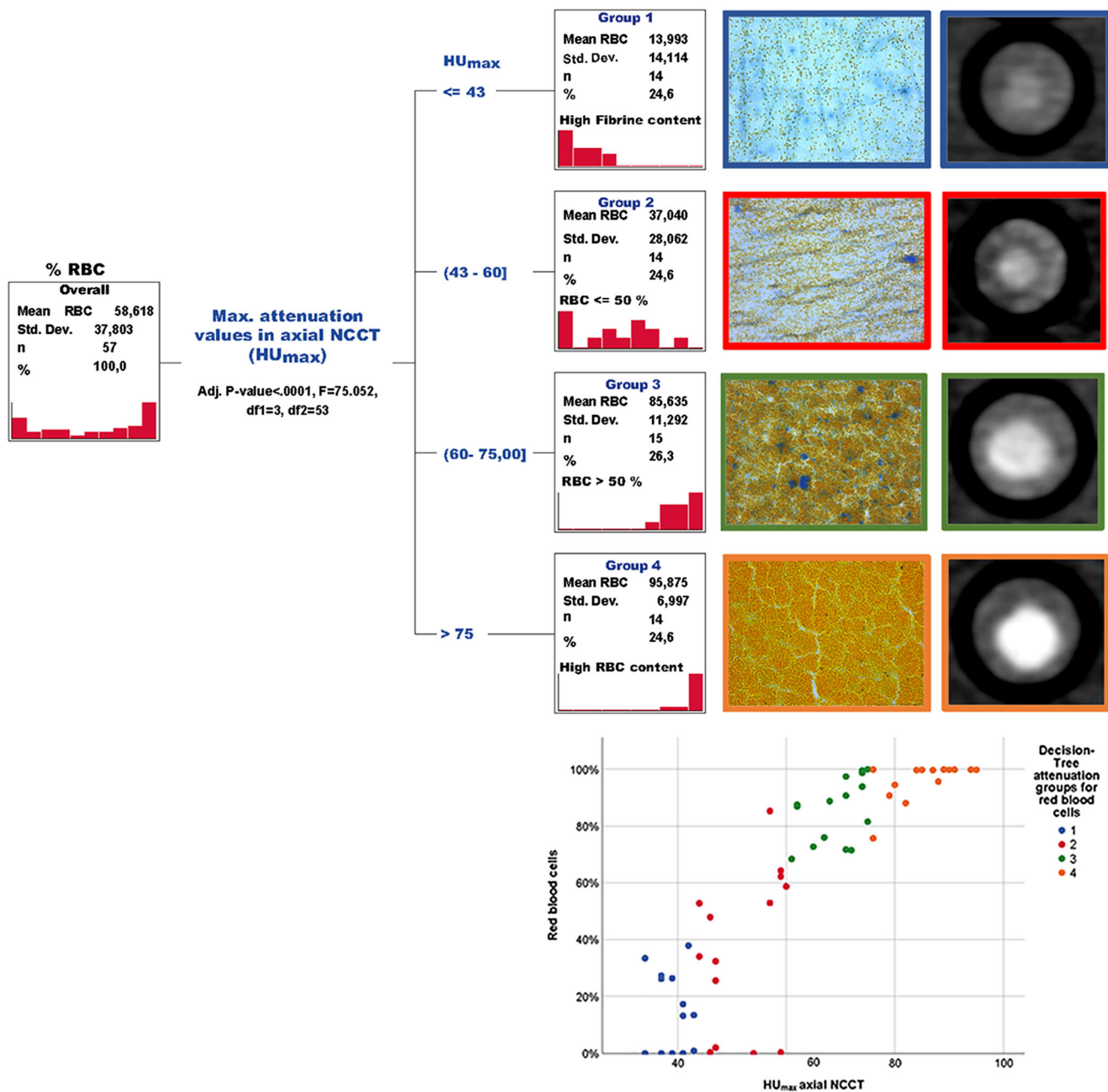


Fig. 2 Decision tree for estimating the percentage red blood cells based on non-contrast CT. This decision tree was used to test six different attenuation parameters (mean, maximum, and minimum attenuation values in axial and coronal reconstructions) as alternatives to determine the one with the most accuracy in predicting the RBC value. The maximum Hounsfield unit (HU) value from the axial reconstructions

was selected. Attenuation cut-offs located at 43 HU, 43–60 HU, 60–75 HU, and >75 HU corresponded with mean RBC values of 14%, 37%, 85%, and 96%. At right, the radiological and histological images (Martius scarlet blue trichrome at × 40 magnification) for each HU group. Below, the RBC distribution and maximum attenuation values with color representations for the final four HU groups

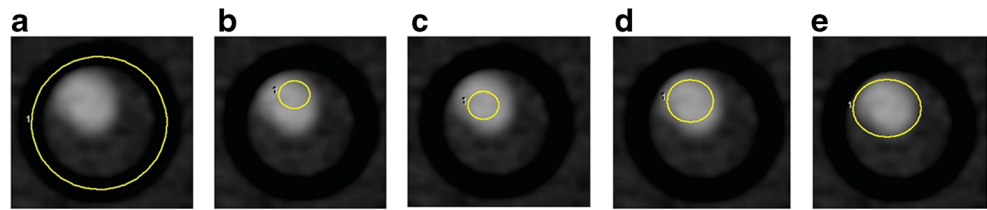
falling within the amplitude of the background noise and, therefore, not clinically significant.

Discussion

This comprehensive study using clot analogs has demonstrated that histology can be correlated with the maximum

attenuation values on axial NCCT. Histologically, there was a nearly perfect inverse correlation between the fibrin and RBC contents. However, by using decision tree algorithms, we were able to define four groups of HU explicitly correlated with the percentage RBCs, which was selected as the most relevant variable affecting attenuation. The iron content was the second factor influencing clot imaging. There was a relatively good linear correlation between the percentage RBCs

Fig. 3 Why maximum attenuation values were better for histological prediction? Example of variations in Hounsfield unit values depending on the size and position of the region of interest on clots. Five examples of ROIs at the same clot level. The table below described the corresponding HU value for each ROI. The maximum attenuation values exhibited no variations with different ROI position and size. This constancy in the maximum HU values might be the reason why the decision tree analysis selected it as a predictor for the percentage RBCs



Hounsfield units values					
Example	ROI area mm ²	Mean	SD	Maximum	Minimum
A	154.2	2.1	36.7	70	-85
B	7.2	62	7.1	70	43
C	7.2	66.6	2.9	70	57
D	16.1	63	5.7	70	46
E	35.4	50.6	15.3	70	12

and the iron content. Nevertheless, clots having a similar high percent of RBCs (90–100%) but different attenuations were identified. Further analysis of this subgroup revealed

substantial differences in iron but also in WBCs, which could explain the variability in clot hyperattenuation. Overall, the water content in the clots varied among the different

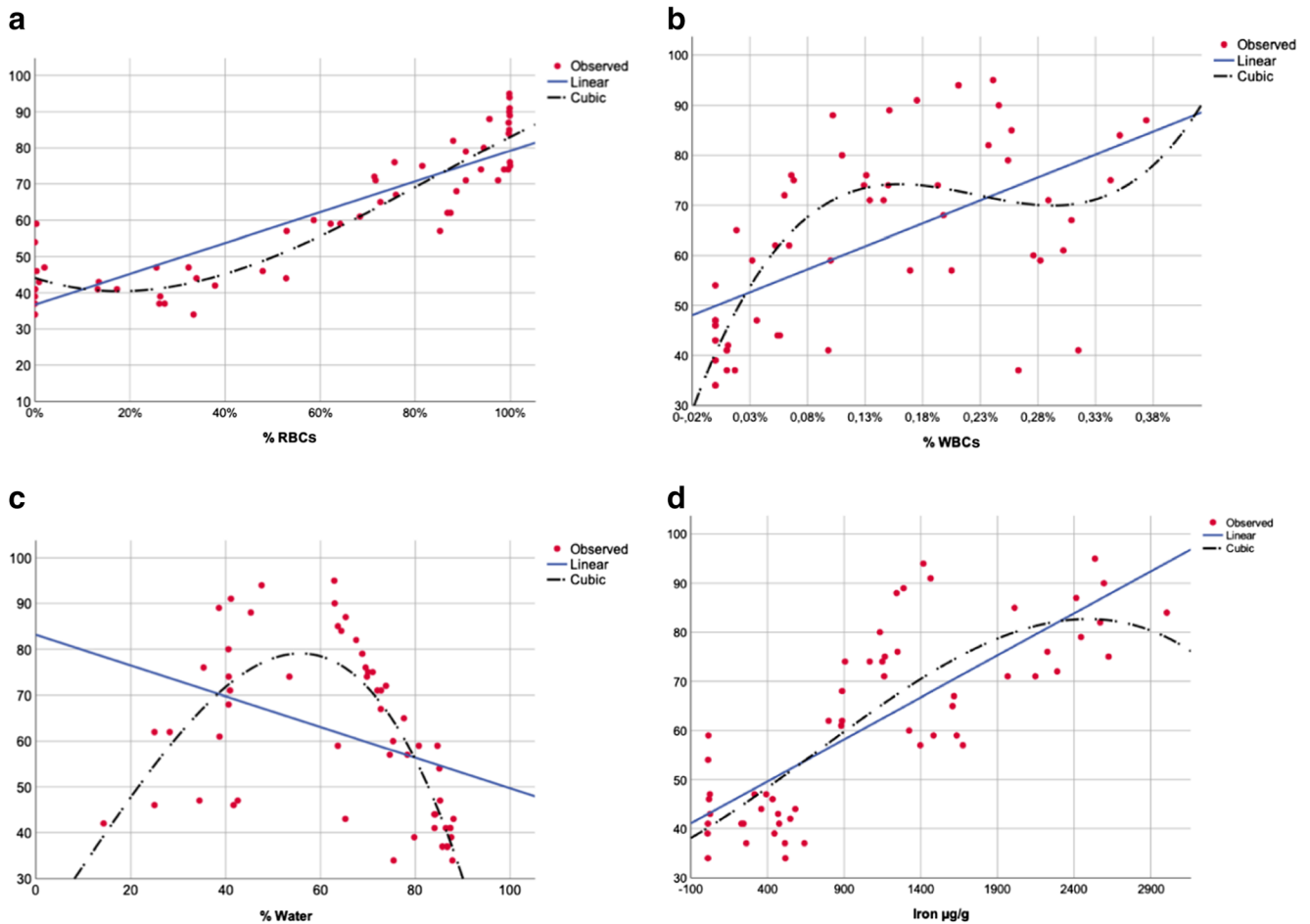


Fig. 4 Relationship of red blood cells (RBCs), white blood cells (WBC)s, iron content, and water content with the maximum attenuation values measured by axial non-contrast CT (NCCT). Regression models were used and compared to identify the optimal mathematical models relating clot attenuation to histological and laboratory analysis

variables. The models with the best fits are shown below. In all cases, with regard to the maximum attenuation values on axial NCCT, the figure depicts the relationship with the **a** percentage RBCs, **b** to the percentage WBCs, **c** to the percentage water, and **d** to the iron content (µg/g)

Table 1 Factors for predicting clot attenuation when linear models and cubic models were used for reference

	% RBCs	<i>p</i> value	% WBCs	<i>p</i> value	Iron (μg/g)	<i>p</i> value	% Water	<i>p</i> value
R^2 linear	0.772	< 0.001	0.340	< 0.001	0.621	< 0.001	0.139	0.004
β_0	36.708		49.870		42.770		83.141	
β_1^a	0.425		91.770		0.017		− 0.335	
R^2 cubic	0.856	< 0.001	0.534	< 0.001	0.655	< 0.001	0.599	0.011
β_0	44.117		40.383		39.942		18.026	
β_1	− 0.432		517.01		0.019		1.429	
β_2	0.014		− 2498.5		5.124E−6		0.008	
β_3	− 5.439E−5		3679.93		− 2.413E−9		− 0.00024	

^a β_1 represents the HU value increment (maximum-axial) per unit by linear regression: 1% of RBCs increased the attenuation of clots by 0.425 points; every 0.5% of WBCs accounted for 45.885 HU; for each 1 μg/g of iron, the HU increased by 0.017 HU; and 1% of water decreased the HU value by 0.335. For the cubic regressions, HU values could be calculated as follows: max HU axial = $\beta_0 + \beta_1 * \text{RBC} + \beta_2 * \text{RBC} * \text{RBC} + \beta_3 * \text{RBC} * \text{RBC} * \text{RBC}$ (example for RBCs)

RBCs red blood cells, WBCs white blood cells, R^2 coefficient of determination, β regression coefficients

histologies. Nevertheless, the multivariate analysis did not show any significant effect on attenuation by water.

Hounsfield units for clots are usually reported as mean values [7, 12, 25]. In this study, we demonstrated that maximum attenuation values from axial NCCT could serve as a better radiological marker of the percentage RBCs than formerly published

mean values. Besides, it was also possible to define up to four attenuation groups predicting histology, and this confirms that meaningful information can be derived from simple NCCT results. RBCs were the most critical factor that contributed to clot density, followed by iron content. It needs to be remembered that, outside histology, the exact thrombus composition remains

Table 2 Differences in the composition of erythrocyte-rich thrombi

Parameter	RBC-rich clots		<i>p</i> value ^a
	Lower attenuation (≤ 80 HU) <i>n</i> = 10	Higher attenuation (> 80 HU) <i>n</i> = 10	
Maximum HU values on axial NCCT			< 0.0001
Mean ± SD	74.2 ± 3.6	88.5 ± 4.2	
Median (IQR)	74 (71–76)	88.5 (85–91)	
Range (min–max)	68–80	82–88.5	
% RBCs			0.16
Mean ± SD	95.4 ± 4.3	98.2 ± 3.8	
Median (IQR)	96 (90.6–99.5)	99.7 (99.6–99.8)	
Range (min–max)	88.7–99.9	88–99.8	
% WBCs			0.019
Mean ± SD	0.15 ± 0.05	0.23 ± 0.08	
Median (IQR)	0.14 (0.13–0.19)	0.24 (0.18–0.26)	
Range (min–max)	0.07–0.25	0.10–0.37	
% Water			0.912
Mean ± SD	53.2 ± 15.3	56 ± 11.3	
Median (IQR)	47 (40.6–70)	63 (45.3–64.3)	
Range (min–max)	35.3–72	38.6–67.5	
Iron (μg/g)			0.023
Mean ± SD	1459 ± 642	2054 ± 652	
Median (IQR)	1156 (1067–1967)	2213 (1417–2570)	
Range (min–max)	887–2625	1224–3005	

^a Mann-Whitney *U* test

RBCs red blood cells, WBCs white blood cells, HU Hounsfield units, NCCT non-contrast CT, SD standard deviation, IQR interquartile range

unknown, and typical hematological values (there is 0.5 mg of iron in 1 ml of blood) cannot be extrapolated. Data on the increase in attenuation by iron are limited when compared, for example, with those for calcium, which has been widely analyzed [26, 27]. Generally speaking, the absorption of radiation depends on the atomic number (Z). Thus, on CT imaging, ferric iron ($Z = 26$) should be still more “dense” than calcium ($Z = 20$). To our knowledge, only one study from 1976 analyzed the attenuation of blood fractions, showing that 1 mg of iron diluted in 100 ml of water contributed 0.0345 EMI units (0.069 HU, $\text{HU} = \text{EMI} \times 2$) [28]. Iron is a component of the hemoglobin protein in erythrocytes, and in this sense, our analysis demonstrated a correlation between RBCs and iron and, still more importantly, between iron and the HU values: every 1 $\mu\text{g/g}$ of iron yields an attenuation of 0.017 HU. However, it should be highlighted that there were significant variations in the iron concentrations (1400–2000 $\mu\text{g/g}$) of RBC-rich clots (95% vs. 98% RBCs), which could explain some of the discrepancies in the attenuation observed. Lastly, we did not find water to have a significant effect on clot imaging when adjusted. The amount of water tended to increase with the fibrin content, which is likely due to the larger interstitial spaces in fibrin-rich clots. On the other hand, as protein polymers, fibrin fibers should contain a significant amount of water since its protein concentration has been estimated at 20% [29]. Similarly, Brown et al. demonstrated that stretching of fibrin clots leads to fiber bundling with a dramatic decrease in volume due to water loss [30]. In summary, there is water inside fibrin clots, and changes in clot morphology, for example, through repetitive interaction with mechanical thrombectomy devices, could lead to water loss and heightened clot stiffness [31].

Clot composition thus alters the physical properties of the thrombi and hence the effectiveness of endovascular recanalization [31–33]. Currently, several endovascular techniques and materials for clot removal are available; some of these have been tested on fibrin-rich clots or with a view to avoiding fragmentation and migration during thrombectomy [22, 34]. This study aimed to discover further insights on clot imaging utilizing NCCT, included in most stroke imaging protocols worldwide. Our analysis has shown that it is possible to find new associations between HU and histology in clot analogs apart from the concept of the hyperdense artery and is intended to serve as a basis for carrying out additional studies in real stroke patients. A positive effect on patient outcomes by implementing stroke therapies based on the clot type to be treated will only be possible if thrombus characterization through imaging significantly improves.

We believe that artificial intelligence has much to contribute to this issue. Even though a considerable amount of data from imaging is required and neuropathology and clinical laboratories will be needed, research should move quickly to discern further patterns based on maximum attenuation values, beyond what meets the eye, so that clot composition

can be reliably estimated from a simple CT. Finally, imaging will serve the purpose not only of stroke diagnosis and patient selection but also of implementing and adjusting stroke therapies in this coming era of more personalized medicine.

Limitations

Our study has several limitations. One limitation of the analysis is the lack of data on the volume and mass of thrombi (density = volume/mass), which influence X-ray absorption and hence attenuation.

Using clot analogs in place of human acute ischemic stroke thrombi is a reliable way to uncover further insights into clot imaging, avoiding the inherent variability of thrombi and the physical impracticalities stemming from their small and irregular size and the significant structural disruption caused by retrieval via thrombectomy. The clot analogs used in this study were made from real blood with tight control of RBC composition to allow repeatability at discrete points over the wide compositional range of human stroke thrombi controlling for interclot and intraclot type variability.

This homogeneous clot analog structure enhanced the accuracy of comparing the results of imaging, clinical laboratory, and neuropathology, and it is an attribute that may occur in real clots. By way of further findings, we have reported four attenuation cut-offs for RBC prediction based on our clot analogs, demonstrating that it is possible to obtain more valuable information from a simple CT. Nevertheless, even when the HU cut-offs from the classification model are reasonable, direct extrapolation of the classification should be taken cautiously in respect of human thrombi in acute ischemic stroke using NCCT. Due to the nature of our experiment, based on absolute maximum HU values for clot analogs, the outcome parameter from the absolute values needs to be adjusted to the clot/contralateral artery HU ratio or to the HU differences between sides, values typically used to characterize AIS thrombi in patients using NCCT. Clot heterogeneity could affect the attenuation and may decrease model performance to a certain extent since the maximum attenuation values from axial reconstructions (and not the average minimum HU) were the ones selected to have the best accuracy for predicting histology.

Besides, due to the production process, clot analogs usually underrepresent the content of WBCs that AIS thrombi should contain. In this analysis, similar RBC-rich thrombi displayed variable imaging associated with different WBC contents. Although a hyperattenuating effect of the WBCs (< 1% in clot analogs) could not be ensured, changes in percentage WBCs in human AIS thrombi could lead to differences in attenuation. This aspect requires further investigation, especially considering the well-known hyperdensity of intracranial lymphomas.

Finally, from a statistical standpoint, the results of decision trees are highly dependent on their construction. In this respect, as noted in the “Methods” section, we preferred to simplify the tree as an aid to being able to draw appropriate generalizations from the training data. Although there was no external validation of the performance of the classification model, the final decision tree for RBC content with a total of four HU groups yielded lower cross-validation error and maximum number of groups for a simple single depth-level classification.

Conclusions

We have demonstrated that it is possible to extract more and valuable information from NCCT that can be extrapolated to provide insights into clot histological and chemical composition. The attenuation of clot analogs depended on large measure, and independently, on both the RBC and iron contents. Beyond the well-known concept of the hyperdense artery, we have demonstrated that it is possible to determine not only hyperdense clots but up to four histological groups based on maximum HU values using non-contrast CT. Thus, this new attenuation classification may be helpful in better understanding which kind of clot we are dealing with prior to initiating any stroke therapy and in opening the door to developing new “clot-targeted” treatments.

Acknowledgments The authors thank the team headed by Dr. Ray McCarthy for providing clot analogs weekly as the source material for our study free of charge. Aglaé Velasco Gonzalez (Neuroradiology) performed this study in collaboration with the Institute of Biostatistics and Clinical Research and Institute of Neuropathology at the Faculty of Medicine, Westfälische Wilhelms-Universität Münster (WWU). We also thank Dr. Senner Volker for coordinating and Mrs. Andrea Rothaus of the neuropathology laboratory for preparing and staining the clot analog samples. Special thanks go to our X-ray technicians who always found a way to complete the experiments on time and whose support was invaluable. Finally, the authors thank the University of Muenster for giving us the time to complete this project.

Compliance with Ethical Standards

Conflict of Interest Aglaé Velasco González performed this study in the context of a program for research backed by the WWU University. One of the authors (Ray McCarthy) is an employee of Cerenovus. Authors who neither advise nor work for the industry had exclusive control over designing and performing the experiment, the data, and data analysis. This study received no industry financial support. All authors have approved the final manuscript.

References

- Campbell BC, Mitchell PJ, Kleinig TJ, Dewey HM, Churilov L, Yassi N, et al. Endovascular therapy for ischemic stroke with perfusion-imaging selection. *N Engl J Med.* 2015;372(11):1009–18.
- Goyal M, Demchuk AM, Menon BK, Eesa M, Rempel JL, Thornton J, et al. Randomized assessment of rapid endovascular treatment of ischemic stroke. *N Engl J Med.* 2015;372(11):1019–30.
- Berkhemer OA, Fransen PS, Beumer D, van den Berg LA, Lingsma HF, Yoo AJ, et al. A randomized trial of intraarterial treatment for acute ischemic stroke. *N Engl J Med.* 2015;372(1):11–20.
- Jovin TG, Chamorro A, Cobo E, de Miquel MA, Molina CA, Rovira A, et al. Thrombectomy within 8 hours after symptom onset in ischemic stroke. *N Engl J Med.* 2015;372(24):2296–306.
- Velasco Gonzalez A, Buerke B, Gorlich D, Chapot R, Smagge L, Velasco MV, et al. Variability in the decision-making process of acute ischemic stroke in difficult clinical and radiological constellations: analysis based on a cross-sectional interview-administered stroke questionnaire. *Eur Radiol.* 2019;29(11):6275–84.
- Niessen JM, van der Schaaf IC, van der Graaf Y, Kappelle LJ, Biessels GJ, Horsch AD, et al. Predictive value of thrombus attenuation on thin-slice non-contrast CT for persistent occlusion after intravenous thrombolysis. *Cerebrovasc Dis.* 2014;37(2):116–22.
- Puig J, Pedraza S, Demchuk A, Daunis IEJ, Termes H, Blasco G, et al. Quantification of thrombus Hounsfield units on noncontrast CT predicts stroke subtype and early recanalization after intravenous recombinant tissue plasminogen activator. *AJNR Am J Neuroradiol.* 2012;33(1):90–6.
- Brinjikji W, Duffy S, Burrows A, Hacke W, Liebeskind D, Majoie C, et al. Correlation of imaging and histopathology of thrombi in acute ischemic stroke with etiology and outcome: a systematic review. *J Neurointerv Surg.* 2017;9(6):529–34.
- Heo JH, Kim K, Yoo J, Kim YD, Nam HS, Kim EY. Computed tomography-based thrombus imaging for the prediction of recanalization after reperfusion therapy in stroke. *J Stroke.* 2017;19(1):40–9.
- Froehler MT, Tateshima S, Duckwiler G, Jahan R, Gonzalez N, Vinuela F, et al. The hyperdense vessel sign on CT predicts successful recanalization with the Merci device in acute ischemic stroke. *J Neurointerv Surg.* 2013;5(4):289–93.
- Mokin M, Morr S, Natarajan SK, Lin N, Snyder KV, Hopkins LN, et al. Thrombus density predicts successful recanalization with Solitaire stent retriever thrombectomy in acute ischemic stroke. *J Neurointerv Surg.* 2015;7(2):104–7.
- Liebeskind DS, Sanossian N, Yong WH, Starkman S, Tsang MP, Moya AL, et al. CT and MRI early vessel signs reflect clot composition in acute stroke. *Stroke.* 2011;42(5):1237–43.
- Moftakhar P, English JD, Cooke DL, Kim WT, Stout C, Smith WS, et al. Density of thrombus on admission CT predicts revascularization efficacy in large vessel occlusion acute ischemic stroke. *Stroke.* 2013;44(1):243–5.
- Mair G, Boyd EV, Chappell FM, von Kummer R, Lindley RI, Sandercock P, et al. Sensitivity and specificity of the hyperdense artery sign for arterial obstruction in acute ischemic stroke. *Stroke.* 2015;46(1):102–7.
- Brouwer PA, Brinjikji W, De Meyer SF. Clot pathophysiology: why is it clinically important? *Neuroimaging Clin N Am.* 2018;28(4):611–23.
- Turk AS 3rd, Campbell JM, Spiotta A, Vargas J, Turner RD, Chaudry MI, et al. An investigation of the cost and benefit of mechanical thrombectomy for endovascular treatment of acute ischemic stroke. *J Neurointerv Surg.* 2014;6(1):77–80.
- Shu L, Meyne J, Jansen O, Jensen-Kondering U. Manual thrombus density measurement depends on the method of thrombus delineation. *J Stroke.* 2018;20(3):411–2.
- Angermaier A, Langner S. Thrombus density measurement is promising but technical standards are needed. *J Neurointerv Surg.* 2017. <https://doi.org/10.1136/neurintsurg-2015-011866>.

19. Bourcier R, Pautre R, Mirza M, Castets C, Darcourt J, Labreuche J, et al. MRI quantitative T2* mapping to predict dominant composition of in vitro thrombus. *AJNR Am J Neuroradiol*. 2019;40(1):59–64.
20. Bretzner M, Lopes R, McCarthy R, Corseaux D, Auger F, Gunning G, et al. Texture parameters of R2* maps are correlated with iron concentration and red blood cells count in clot analogs: a 7T micro-MRI study. *J Neuroradiol*. 2019. <https://doi.org/10.1136/j.neurad.2019.10.004>.
21. Janot K, Oliveira TR, Fromont-Hankard G, Annan M, Filipiak I, Barantin L, et al. Quantitative estimation of thrombus-erythrocytes using MRI. A phantom study with clot analogs and analysis by statistic regression models. *J Neurointerv Surg*. 2019. <https://doi.org/10.1136/neurintsurg-2019-014950>.
22. Fennell VS, Setlur Nagesh SV, Meess KM, Gutierrez L, James RH, Springer ME, et al. What to do about fibrin rich ‘tough clots’? Comparing the Solitaire stent retriever with a novel geometric clot extractor in an in vitro stroke model. *J Neurointerv Surg*. 2018;10(9):907–10.
23. Johnson S, Duffy S, Gunning G, Gilvarry M, McGarry JP, McHugh PE. Review of mechanical testing and modelling of thrombus material for vascular implant and device design. *Ann Biomed Eng*. 2017;45(11):2494–508.
24. Duffy S, Farrell M, McArdle K, Thornton J, Vale D, Rainsford E, et al. Novel methodology to replicate clot analogs with diverse composition in acute ischemic stroke. *J Neurointerv Surg*. 2017;9(5):486–91.
25. Brinjikji W, Michalak G, Kadirvel R, Dai D, Gilvarry M, Duffy S, et al. Utility of single-energy and dual-energy computed tomography in clot characterization: an in-vitro study. *Interv Neuroradiol*. 2017;23(3):279–84.
26. Cecchin E, De Marchi S, Querin F, Marin MG, Fiorentino R, Tesio F. Efficacy of hepatic computed tomography to detect iron overload in chronic hemodialysis. *Kidney Int*. 1990;37(3):943–50.
27. Jang S, Graffy PM, Ziemlewicz TJ, Lee SJ, Summers RM, Pickhardt PJ. Opportunistic osteoporosis screening at routine abdominal and thoracic CT: normative L1 trabecular attenuation values in more than 20 000 adults. *Radiology*. 2019;291(2):360–7.
28. New PF, Aronow S. Attenuation measurements of whole blood and blood fractions in computed tomography. *Radiology*. 1976;121(3 Pt. 1):635–40.
29. Voter WA, Lucaveche C, Erickson HP. Concentration of protein in fibrin fibers and fibrinogen polymers determined by refractive index matching. *Biopolymers*. 1986;25(12):2375–84.
30. Brown AE, Litvinov RI, Discher DE, Purohit PK, Weisel JW. Multiscale mechanics of fibrin polymer: gel stretching with protein unfolding and loss of water. *Science*. 2009;325(5941):741–4.
31. Gunning GM, McArdle K, Mirza M, Duffy S, Gilvarry M, Brouwer PA. Clot friction variation with fibrin content; implications for resistance to thrombectomy. *J Neurointerv Surg*. 2018;10(1):34–8.
32. Weafer FM, Duffy S, Machado I, Gunning G, Mordasini P, Roche E, et al. Characterization of strut indentation during mechanical thrombectomy in acute ischemic stroke clot analogs. *J Neurointerv Surg*. 2019;11:891–7.
33. van der Marel K, Chueh JY, Brooks OW, King RM, Marosfoi MG, Langan ET, et al. Quantitative assessment of device-clot interaction for stent retriever thrombectomy. *J Neurointerv Surg*. 2016;8(12):1278–82.
34. Chueh JY, Kuhn AL, Puri AS, Wilson SD, Wakhloo AK, Gounis MJ. Reduction in distal emboli with proximal flow control during mechanical thrombectomy: a quantitative in vitro study. *Stroke*. 2013;44(5):1396–401.

Publisher's Note Springer Nature remains neutral with regard to jurisdictional claims in published maps and institutional affiliations.

Affiliations

Aglae Velasco Gonzalez¹  · Boris Buerke¹ · Dennis Görlich² · Manfred Fobker³ · Thilo Rusche¹ · Cristina Sauerland² · Norbert Meier⁴ · Astrid Jeibmann⁵ · Ray McCarthy⁶ · Harald Kugel⁴ · Peter Sporns¹ · Andreas Faldum² · Werner Paulus⁵ · Walter Heindel¹

¹ Department of Clinical Radiology, Neuroradiology, University Hospital Muenster, Albert-Schweitzer-Campus 1, Gebäude A1, 48149 Muenster, Germany

² Institute of Biostatistics and Clinical Research, University of Muenster, Schmeddingstraße 56, 48149 Muenster, Germany

³ Center for Laboratory Medicine, University Hospital Muenster, Albert-Schweitzer-Campus 1, Gebäude A1, 48149 Muenster, Germany

⁴ Department of Clinical Radiology, Medical Physics, University Hospital Muenster, Albert-Schweitzer-Campus 1, Gebäude A1, 48149 Muenster, Germany

⁵ Institute of Neuropathology, University Hospital Muenster, Pottkamp 2, 48149 Muenster, Germany

⁶ Cerenovus, Galway Neuro Technology Centre, Mervue Business Park, Galway, Ireland